communications biology

Article

https://doi.org/10.1038/s42003-024-06774-6

Inhibition of falcilysin from *Plasmodium falciparum* by interference with its closed-to-open dynamic transition

Check for updates

Jianqing Lin[1,2], Xinfu Yan[1,2], Zara Chung[1,2], Chong Wai Liew[1,2], Abbas El Sahili[1,2], Evgeniya V. Pechnikova[3,5], Peter R. Preiser[1,4], Zbynek Bozdech[1,2], Yong-Gui Gao[1,2] & Julien Lescar[1,2,4] ✉

In the absence of an efficacious vaccine, chemotherapy remains crucial to prevent and treat malaria. Given its key role in haemoglobin degradation, falcilysin constitutes an attractive target. Here, we reveal the mechanism of enzymatic inhibition of falcilysin by MK-4815, an investigational new drug with potent antimalarial activity. Using X-ray crystallography, we determine two binary complexes of falcilysin in a closed state, bound with peptide substrates from the haemoglobin α and β chains respectively. An antiparallel β-sheet is formed between the substrate and enzyme, accounting for sequence-independent recognition at positions P2 and P1. In contrast, numerous contacts favor tyrosine and phenylalanine at the P1' position of the substrate. Cryo-EM studies reveal a majority of unbound falcilysin molecules adopting an open conformation. Addition of MK-4815 shifts about two-thirds of falcilysin molecules to a closed state. These structures give atomic level pictures of the proteolytic cycle, in which falcilysin interconverts between a closed state conducive to proteolysis, and an open conformation amenable to substrate diffusion and products release. MK-4815 and quinolines bind to an allosteric pocket next to a hinge region of falcilysin and hinders this dynamic transition. These data should inform the design of potent inhibitors of falcilysin to combat malaria.

In total, 247 million cases of malaria were recorded in 2021, and about half a million people die of the disease every year[1]. The continuous decrease in malaria cases and deaths observed in the last two decades is now slowing down[1]. No vaccine is widely available yet, although several candidates have been tentatively deployed[2]. Malaria prevention, treatment, and containment largely rely on controlling the mosquito vector and on chemotherapy. The situation is aggravated by the emergence of parasites resistant to artemisinin-based combination therapies that include—in addition to dihydro-artemisinin—a longer half-life partner drug such as lumefantrine, piperaquine or mefloquine[3,4]. The emergence of parasites resistant to commonly used drugs has triggered concerted efforts to collect chemical compounds showing promising efficacy in phenotypic cell-based assays[5]. These compounds have been included in repositories such as the "Medicine for Malaria Venture"[6]. In many cases, though, their mode of action remains poorly defined[7,8].

MK-4815 is a small molecule with promising antimalarial activity and a good pharmacokinetics profile in mice and rhesus monkeys[9]. This drug candidate was identified using an in vitro erythrocytic stage assay of *Plasmodium falciparum* replication. MK-4815 accumulates in infected red blood cells and is effective against the late trophozoite and early schizont stages of the parasite. In addition to the wild-type parasite, several documented drug-resistant field isolates of *P. falciparum* were also sensitive to treatment with MK-4815. In a *Plasmodium berghei* mouse model of malaria, whereas untreated animals die about 10 days post-infection, treatment with MK-4815 with a total dose of 50 mg/kg led to a cure. Given its attractive profile, MK-4815 represents an orally active molecule that could be used in combination therapy to treat malaria[9].

To better understand the mechanism of actions of existing and candidate antimalarial drugs such as MK-4815, we performed target deconvolution studies using the cellular thermal shift assay coupled with

[1]School of Biological Sciences, Nanyang Technological University, 60 Nanyang Drive, 637551 Singapore, Singapore. [2]NTU Institute of Structural Biology, Nanyang Technological University, Experimental Medicine Building (EMB), 59 Nanyang Drive, Level 06-01, 636921 Singapore, Singapore. [3]Materials and Structural Analysis Division, Thermo Fisher Scientific, Eindhoven, Netherlands. [4]Antimicrobial Resistance Interdisciplinary Research Group, Singapore-MIT Alliance for Research and Technology Centre, 1 CREATE Way, 138602 Singapore, Singapore. [5]Present address: Dens Solutions, Informaticalaan 12, 2628 ZD Delft, Netherlands. ✉e-mail: julien@ntu.edu.sg

mass spectrometry (MS-CETSA)[10–13]. Using MS-CETSA, we identified the purine nucleoside phosphorylase from *P. falciparum* as a target of several quinolines and of MMV000848[11,13]. Falcilysin (FLN) was identified as a promiscuous target of MMV000848, several quinoline drugs such as chloroquine and mefloquine, and also of MK-4815[11]. Co-crystal structures of FLN bound to quinolines and to MK-4815 revealed a putative allosteric binding pocket distant from the protease active site[11].

FLN is a large (Mr 139 kDa) zinc metalloprotease of the M16C family that mediates hemoglobin degradation in the digestive vacuole (DV)[14,15]. FLN cleaves small oligopeptides that are proteolytic products of other upstream haemoglobinases such as falcipains, plasmepsins, and histoaspartate (HAP) proteases[16,17]. During its catalytic cycle, FLN first adopts an open conformation allowing substrate diffusion into its large catalytic chamber. Next, the protease adopts a closed state conducive to substrate proteolysis, and finally, the enzyme reopens, releasing cleaved products. The detailed molecular features of this cycle are not known for FLN.

FLN has a preference for 11–15 amino acid-long peptides rich in bulky and charged residues. Substrates have a polar or charged residue at P1 position, a charged residue at P2, and an aromatic residue at P1', but overall, the structural basis for peptide recognition by FLN remains elusive[16]. FLN carries inverted "HXXEH" motifs at its active site, a characteristic shared by several M16 proteases found in plants[18]. Two *Arabidopsis* endopeptidase, PreP1 and PreP2, are phylogenetically close ancestors of FLN responsible for degrading transit/targeting peptides in the chloroplast and mitochondria[19]. FLN also accumulates in the *Plasmodium* apicoplast, the endosymbiotic analog of chloroplast, and, to a lesser degree, in the mitochondrion[17]. In the apicoplast, FLN cleaves free signal transit peptides from over 400 nuclear proteins essential for the parasite metabolism, such as for fatty acid type II synthesis, non-mevalonate isoprenoid synthesis, heme synthesis, and iron-sulfur cluster assembly[20]. Thus, FLN accumulation in the plastid or mitochondria may represent the ancestral localization of this enzyme, while its presence in the DV could constitute an evolutionary diversion in the trafficking process via the endocytic pathway[17]. Either in its DV or apicoplast locations, FLN functions as an endopeptidase, mediating organellar "clearance" of short polypeptides. FLN inhibition leads to massive accumulations of short polypeptides that disrupt the normal function of these organelles and, as a result, lead to parasite death. Inhibition of FLN in the DV disrupts hemoglobin proteolysis, blocking the release of hemoglobin-derived amino acids that represent a major metabolic source for *Plasmodium* parasite during its asexual development[21].

Among compounds imparting thermal stability to FLN, MK-4815 binds to FLN most tightly, with a dissociation constant K_d of 1.79 μM. MK-4815 displays the strongest enzymatic inhibition with an IC_{50} value of 1.61 μM at pH 7.5[11]. In a killing assay using a parasite with partial knockdown of FLN expression, a decrease in the EC_{50} value of MK-4815 correlated with a decrease in FLN expression. MK-4815 binds to a pocket of FLN located ~24 Å away from the metalloprotease active site[11]. This pocket is lined by residues Phe82, Phe527, Ile544, and Phe545, that form a hydrophobic patch at the surface of the FLN catalytic chamber. Other drugs such as quinoline or MMV000848 also bind to this pocket largely exposed to the solvent[11]. A Lineweaver–Burk plot showed that MK-4815 uses a non-competitive inhibition mechanism to inhibit FLN[11]. Biophysical, enzymatic, and genetic evidence points to a degree of involvement of FLN in the mechanism of action of MK-4815 in killing the parasite.

Given FLN essentiality in the parasite life cycle, FLN appears as a promising drug target against malaria, although no drug specifically targeting this enzyme is available yet. Here we decided to explore how MK-4815 and quinoline drugs inhibit FLN using a combination of structural methods. The data reveal at the atomic level (i) how FLN recognizes its hemoglobin peptide substrates, (ii) structural changes that occur during the catalytic cycle, and (iii) suggest a mechanism for how MK-4815 and—by analogy, quinolines—inhibit the proteolytic activity of FLN.

Results

Crystal structures of falcilysin bound to hemoglobin peptide substrates

A schematic view of the FLN amino-acid sequence and domain organization is given in Fig. 1A. FLN can be broken into a N-terminal half ("N-half") spanning residues 1–630 and a C-terminal half ("C-half", residues 651–1193). Residues 631–650, which comprise two short helical segments, link these two domains in a flexible way, as detailed below (Fig. 1B). The FLN active site comprises a catalytic zinc ion coordinated by H129, H133, and E243. Mixing FLN with peptide substrates leads to cleavage and our initial attempts to co-crystallize wild-type FLN with peptides resulted in FLN crystals devoid of substrates or products. To capture a complex in the pre-cleavage, substrate-bound state of the catalytic cycle, we generated a proteolytically inactive mutant by mutating the general acid/base catalytic residue E132 of FLN to glutamine ("E132Q" single FLN mutant). We were able to co-crystallize this E132Q inactive mutant with two previously reported hemoglobin peptide substrates[14] comprising residues L34 to D47 of the α chain and V33 to D47 of the β chain and determined their structures at 1.86 Å and 2.3 Å resolution, respectively (Table 1, Fig. 2). Hereafter, we name these two peptide substrates "α-peptide" and "β-peptide" respectively. Residues K40 to P44 of the α-peptide (Fig. 2A) and T38 to E43 of the β-peptide (Fig. 2B) could be built unambiguously in the electron density maps (Fig. 2C). Only weak density was visible for residues L34–T39 (α-peptide) and for the C-termini of both peptides suggesting flexibility of these segments.

In the FLN co-crystal structures bound with the hemoglobin α- and β- peptide, a large inner catalytic chamber accommodates the peptide substrates. This chamber, which has a total volume of 10,886 $Å^3$ is created by N-half abutting the C-half, constituting the closed form of FLN (Fig. 2A, B). Overall, five residues of the α-peptide are ordered with an average temperature factor of 53.3 $Å^2$, while six residues out of fifteen are visible for the bound β-peptide with an average temperature factor of 56.2 $Å^2$ (Fig. 2 and Table 1). Importantly, in the vicinity of the FLN active site, the bound α- and β-peptides adopt a common horseshoe-like conformation within the catalytic chamber: a r.m.s deviation of 0.20 Å is observed for the C_α atoms of the five residues that could be superimposed (Fig. 2C). Of note, in the native hemoglobin 3D structure, the corresponding segments belong to two α-helices connected by a bend, which shows that FLN recognizes a non-natively folded state of the substrate. This observation is consistent with the putative downstream role of FLN to only cleave fragments of hemoglobin that are proteolytic products of upstream *Plasmodium* proteases[16,17].

Distances between the amino and carboxy termini of the ordered residues of the α- and β-peptides are 11.0 Å and 12.6 Å, respectively. Visible residues occupy total volumes of 688 $Å^3$ and 869 $Å^3$, respectively, which represent only about 6.3% and 8% of the total volume of the catalytic chamber, respectively. Residues from both the N-half and C-half of FLN make interactions with the peptides (Fig. 2C–E). Electrostatics surfaces display a negative potential in the N-half chamber and an overall positive potential in the C-half chamber (Fig. 2E). Starting from an open state, these oppositely charged surfaces are likely to help bring together the N-half and C-half of the enzyme to form a closed state capable of fully encasing the peptide substrate, conducive to proteolysis.

To examine whether peptide binding to FLN could provoke direct steric hindrance with the MK-4815 inhibitor, we compared the peptide-FLN binary complexes with previously reported structures of inhibitors bound to FLN[11]: these inhibitors bind to a common hydrophobic pocket in the N-half of FLN located at a distance of about 24 Å from the catalytic zinc ion. A superimposition of the binary complexes of FLN bound with MK-4815 and the hemoglobin peptides is shown in Fig. 2D. This overlay shows that the nearest distance between MK-4815 and the ordered part of the peptide substrates is 18.7 Å to residue K40 of α-peptide and 15.5 Å to residue T38 of β-peptide (Fig. 2D). This observation rules out direct competition between the inhibitor and substrate and indicates an allosteric mode of inhibition.

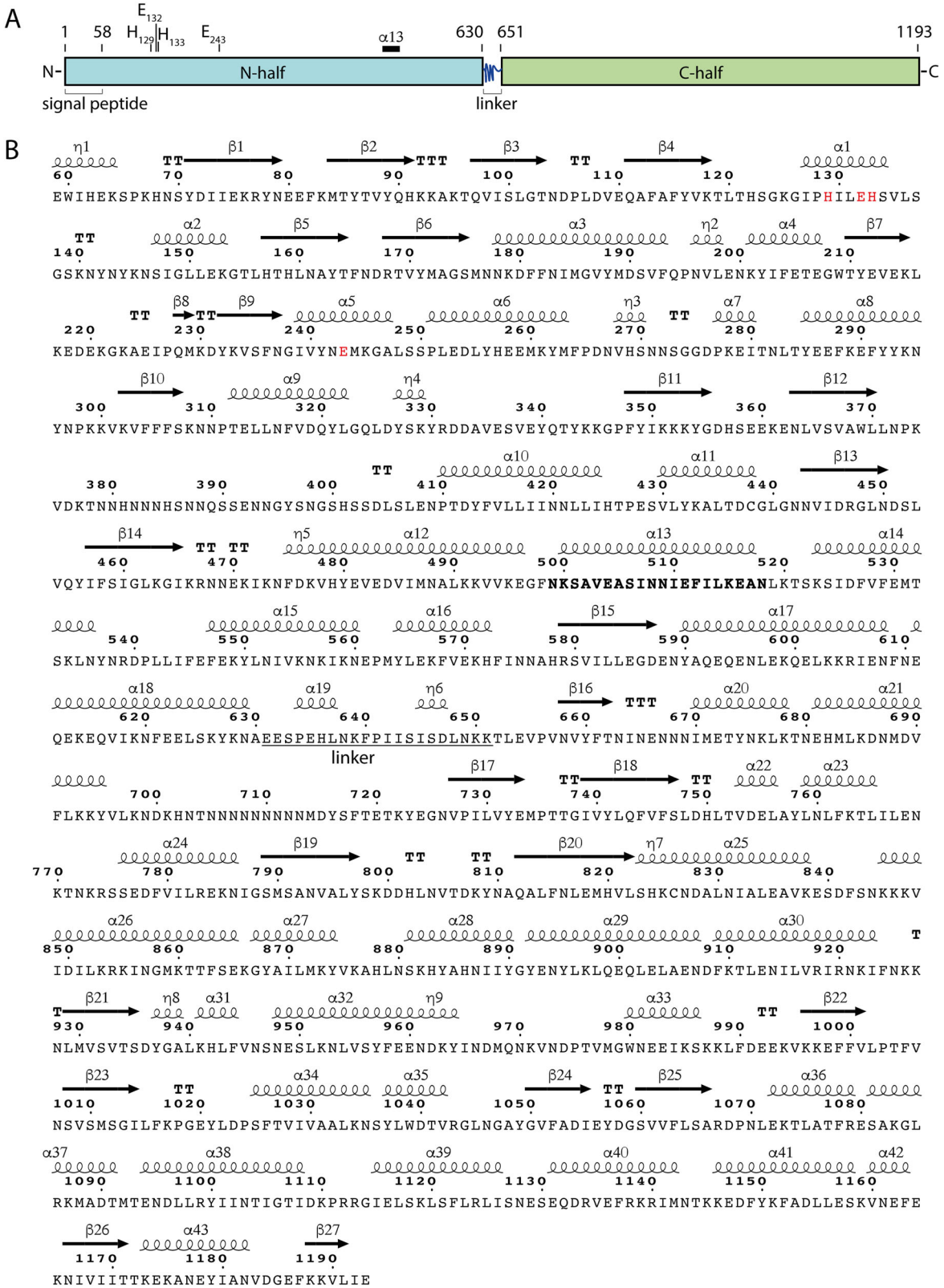

Fig. 1 | Falcilysin domain and sequence structure. A Schematic representation of FLN domain structure with catalytic residues labeled. Helix α13, proposed to act as a hinge region in the open-to-closed transition, is labeled. **B** Amino-acid sequence of FLN with the secondary structure displayed on top of the sequence. The catalytic residue E132, as well as zinc-coordinating residues H129, H133, and E243, are colored in red. Residues from helix α13 are in bold. Linker residues connecting N-half and C-half are underlined. The figure was generated using ESPript. *η*: 3_{10}-helix, TT: β-turn and TTT: α turn.

Table 1 | Data collection and refinement statistics of crystals of falcilysin complexed with peptide substrates derived from the hemoglobin α- and β-chains

	Falcilysin E132Q α-peptide complex	Falcilysin E132Q β-peptide complex
Data collection		
Space group	$P2_12_12_1$	$P2_12_12_1$
Cell dimensions		
a, *b*, *c* (Å)	94.12, 105.72, 125.36	94.09, 105.87, 114.91
α, β, γ (°)	90, 90, 90	90, 90, 90
Resolution (Å)[a]	50.00–1.86 (1.93–1.86)	50.00–2.30 (2.38–2.30)
R_{merge}[b]	0.088 (1.402)	0.143 (0.903)
$I / \sigma I$	19.10 (1.79)	10.30 (2.23)
$CC_{1/2}$	0.999 (0.771)	0.996 (0.748)
Completeness (%)	99.90 (99.17)	99.91 (99.90)
Redundancy	13.7 (13.7)	7.4 (7.1)
Refinement		
Resolution (Å)	46.09–1.86	48.08–2.30
No. of reflections	1,04,687 (10,280)	51,607 (5041)
R_{work}/R_{free}[c,d]	0.189/0.210	0.205/0.251
No. of atoms		
Protein	8881	8886
Peptide	46	58
Water	764	301
B-factors (Å^2)		
Protein	37.18	41.47
Peptide	53.29	56.17
Water	43.50	46.38
R.m.s. deviations		
Bond lengths (Å)	0.010	0.006
Bond angles (°)	1.26	0.81
PDB accession codes	8WXW	8WXZ

[a]Statistics for the highest-resolution shell are shown in parentheses.
[b]$R_{merge} = \Sigma_h\Sigma_i|I_{hi} - \langle I_h\rangle|/\Sigma_{h,i}\, I_{hi}$, where I_{hi} is the ith observation of the reflection *h*, while $\langle I_h\rangle$ is its mean intensity.
[c]$R_{work} = \Sigma||F_{obs}| - |F_{calc}||/\Sigma|F_{obs}|$. Calculated over 95% of reflections.
[d]R_{free} was calculated with 5% of reflections excluded from the whole refinement procedure.

Specificity of hemoglobin substrate recognition by falcilysin

Despite its very large catalytic chamber, FLN is unable to cleave the complete hemoglobin protein or denatured globin polypeptides and preferentially cleaves peptides that are intermediate products of hemoglobin degradation[16]. An alignment of the amino-acid sequences of the α- and β-peptides based on their common orientation in the binary complexes is shown in Fig. 3A. The most noticeable feature is the formation of a β-strand by residues P2 to P1' of the peptide substrates, which form an antiparallel β-sheet with strand β5 of FLN (Fig. 3B, C). The (Φ,Ψ) angles observed for residues at positions P2 and P1 are close to typical values observed for antiparallel β-strands[22] (Fig. S1). At position P1', while the Φ angles fall within the range observed for typical β-strands, the Ψ angles are -45.62° for the α-peptide and -39.17° for the β-peptide, thus ending the β-strand. Both the amino and carbonyl groups of residues P2' establish hydrogen bonds with the side chain of N161. This pattern of substrate recognition appears to be a general feature in M16 metalloproteases: An antiparallel β-sheet with the peptide substrate was observed in other M16 metalloproteases bound to their substrates, such as in the yeast mitochondrial processing peptidase[19], the human insulin-degrading enzyme[23], and the *Arabidopsis thaliana* pre-sequence protease[24]. In contrast, the human pre-sequence protease was reported to form a parallel β-sheet with its peptide substrate[25].

The P1–P1' peptide cleavage sites are T41–Y42 for the α-peptide and R40–F41 for the β-peptide. The corresponding scissile amide bonds are brought in close proximity with the Q132 sidechain (E132 in the wild-type enzyme) via the precise positioning of the substrate afforded by the formation of an antiparallel β-sheet (Fig. 3B, C). Structure-based alignment allowed us to unambiguously assign residues P8 to P6' revealing some conserved residues between both substrates: leucine or valine are found at position P8, phenylalanine or tyrosine at P6, proline at P5, threonine at P3. Position P1 is occupied by threonine and arginine in the α- and β-peptide, respectively, with polar contacts established by the corresponding sidechains (Fig. 3A, B). On the prime side of the cleavage site, tyrosine (Y42) or phenylalanine (F41) are found at P1', and a phenylalanine is strictly conserved at positions P2' and P5' (Fig. 3A). An extensive network of interactions between the P1' residue and residue R1043 from FLN appears crucial for conferring specificity to peptide recognition: R1043 forms a cation-π interaction with the aromatic groups of Y42 (α-peptide) and F41 (β-peptide) respectively (Fig. 3B, C). Hydrogen bonds are also observed between the guanidinium side chain of R1043 with the P1' backbone carbonyl group, between the P1' main chain amine group and the carbonyl oxygen atom of A162 (Fig. 3B, C), and between the hydroxyl group of Y42 with the side chain of N146 (Fig. 3B). The requirement for phenylalanine at P2' appears to derive from the conformation of the substrate which is stabilized in part via intramolecular contacts between the aromatic rings of the P1' and P2' residues (Fig. 3B, C).

To test the importance of these interactions identified via crystallography for substrate recognition, we examined the impact of the N161A and R1043A mutations both on substrate binding and enzyme activity. Compared to the E132Q FLN single mutant, which binds to the α-peptide with a K_d of 933 nM and to the β-peptide with a K_d of 499 nM, the E132Q/N161A and E132Q/R1043A double mutants do not bind the hemoglobin peptides (Fig. S2). Consistently, the enzyme activity of wild-type FLN is abolished by the N161A mutation or the R1043A mutation (Fig. S3), further demonstrating the essential roles of N161 and R1043 in stabilizing the interaction between FLN and the α- and β-peptides.

Thermostabilization of FLN in the presence of the hemoglobin peptides was observed using differential scanning fluorimetry: the presence of 200 μM α-peptide and β-peptide increases the thermal stability of FLN by 7.1 °C and 5.6 °C, respectively (Fig. S4A). These values are higher compared with thermal stabilization imparted by the MK-4815 inhibitor: upon binding MK-4815, the stability of FLN is increased by 2.2 °C (Fig. S4B).

Catalytic mechanism and conformation of the active site

The carbonyl carbon atom of the P1 residue of hemoglobin α- and β-peptide is located 4.4 Å and 4.1 Å away, respectively, from Q132 of the FLN single mutant (Fig. 3D, E). Although both distances are in agreement with the accepted catalytic mechanism for mono-metallic metallopeptidases[18], the zinc coordination differs between the two complexes. In the FLN α-peptide complex, the zinc ion is tetrahedrally coordinated by H129, H133, E243, and a water molecule with the latter also forming two hydrogen bonds with the backbone of α-peptide (Fig. 3D). In contrast, in the FLN β-peptide complex, the water molecule coordinating the zinc ion is absent (Fig. 3E). Instead, the fourth zinc coordinating atom is contributed by the carbonyl oxygen atom of the scissile amide bond (Fig. 3E). Structural superimposition of the two binary complexes reveals a slightly more closed conformation in the complex with the β-peptide compared to the α-peptide (Fig. 3F). This quaternary movement with an overall r.m.s deviation of 1.60 Å, is accompanied by a shift of the zinc ion towards the β-peptide and of zinc-coordinating residues H129, H133, E243, as seen in a magnified view of the active site (Fig. 3G). As a result, the distance between the zinc ion and the β-peptide carbonyl group is reduced from 4 Å to only 2 Å. Hereafter, we will refer to the conformations of FLN in the α-peptide complex as closed conformation 1 ("C1" state) and

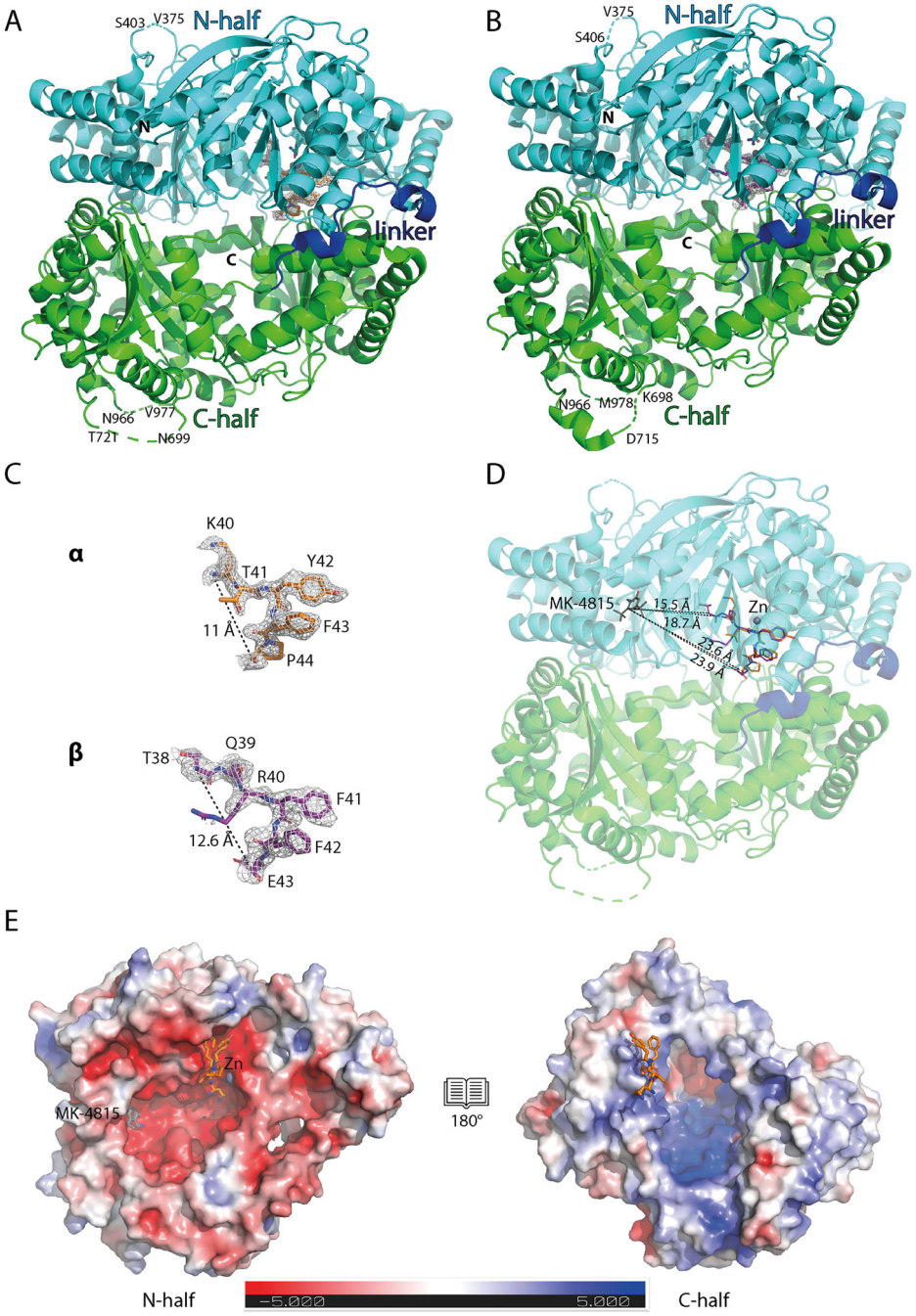

Fig. 2 | Co-crystal structures of FLN in complex with two hemoglobin peptide substrates. A FLN in complex with the hemoglobin α-peptide. Residues K40 to P44 could be built with confidence and are displayed as sticks colored in orange. **B** FLN in complex with the hemoglobin β-peptide. Residues T38 to E43 are colored in purple. Overlayed are F_o–F_c electron density difference Fourier maps where the peptides were omitted from calculation, displayed as mesh, and contoured at 2σ level above the mean. The zinc ion is shown as a gray sphere, and zinc-coordinating residues as cyan sticks. The N-terminus and C-terminus of FLN are labeled in bold. The N-terminal half of FLN is colored in cyan, its C-terminal half in green; linker connecting the two halves is blue. **C** magnified views of the α- and β-peptides with the "omit" electron density maps calculated as in panels (**A**) and (**B**). **D** Superposition of FLN-MK-4815 complex structure (PDB accession code: 7DIJ) with the FLN-α- and β-peptide complex structures. Distances between the drug and each peptide are indicated. MK-4815 is depicted as gray sticks. **E** Display of FLN electrostatics molecular surface for its N-half and C-half. Peptide substrate from hemoglobin α chain and MK-4815 are shown as sticks and zinc ion as a gray sphere.

in the β-peptide complex as closed conformation 2 ("C2" state). A slight opening of FLN when adopting its "C2" state by a rotation of approximately 4.4° would suffice to switch to the "C1" state (Fig. 3F and Supplementary Video 1). In addition, the difference in conformation between the "C1" and "C2" states was also reflected in the corresponding unit cell dimensions, with the slightly more compact "C2" state crystallizing with a smaller c-axis dimension (Table 1). Searching structures deposited with the PDB and based on r.m.s deviations between superimposed structures (Table 2), we found that the "C2" conformation was only observed in a free FLN structure (PDB accession code: 3S5K), while the "C1" conformation was observed in several FLN crystal structures, including free FLN structures (PDB accession codes: 3S5I, 3S5H, 3S5M) and FLN-inhibitor complexes (PDB accession codes: 7VPE, 7DI7, 7DIA, 7DIJ, 8HO4, 8HO5). However, the biological relevance of the existence of two closed conformations in various crystal structures of FLN remains uncertain. Here, through a comparison between the FLN-α and β-peptide complexes, we found that an apparently minor overall conformational difference between the "C1" and "C2" states is accompanied by a significant difference in zinc coordination network at the FLN active site: In the catalytic mechanism of mono-metallic peptidases, direct binding of the carbonyl oxygen from the scissile bond to zinc is essential for Michaelis complex formation. The zinc ion helps to polarize the oxygen atom so that the carbonyl carbon becomes susceptible to nucleophilic attack by a solvent molecule. Hence, the "C2" state observed in the β-peptide complex likely represents a catalytically active closed state of FLN, while the "C1" state observed in the α-peptide complex possibly constitutes an inactive closed state, because the zinc is not directly coordinated by the carbonyl oxygen of the scissile peptide bond.

Having observed two distinct closed conformations, "C1" and "C2" in FLN-hemoglobin peptide binary complexes, we next explored the open forms of FLN. We also examined the impact of the allosteric

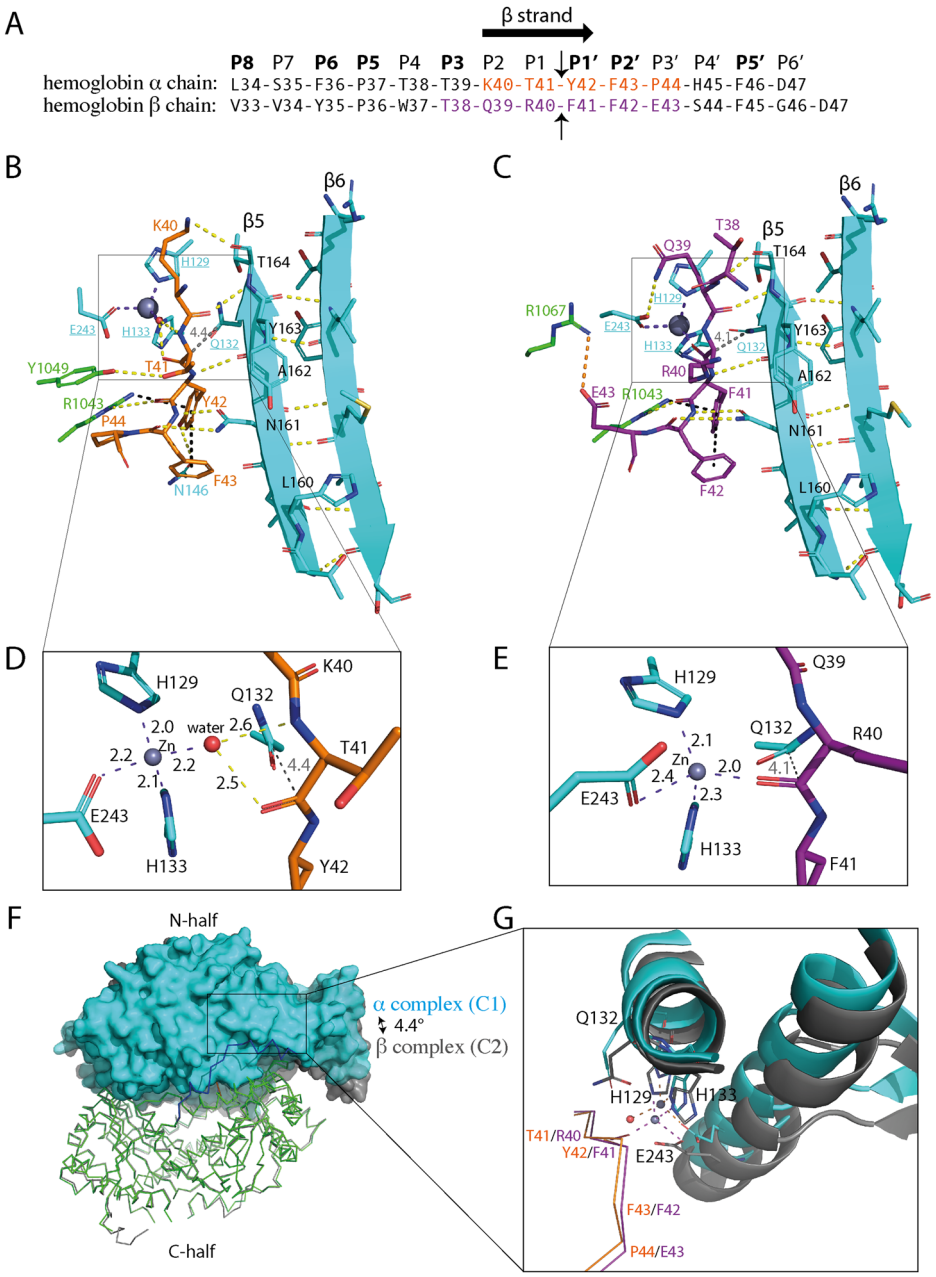

Fig. 3 | Falcilysin-peptide substrates interactions. **A** Amino-acid sequence alignment of the hemoglobin α- and β-peptides. Residues that could be built in clear electron density are colored in orange and purple for the α- and β-peptide respectively. Vertical arrows indicate proteolytic cleavage site by FLN. Substrate positions having either conserved or chemically similar amino acids are shown in bold. Residues at P2, P1, and P1' positions form a β strand. **B**, **C** Detailed view of the interactions between FLN and the hemoglobin α-peptide (**B**) and β-peptide (**C**). Hydrogen bonds are displayed as yellow dashes; cation–π and π–π interactions as black dashes; salt bridge: orange dash; zinc-coordination: purple dashes. Residues K40, T41, and Y42 of α-peptide (panel **B**) and residues Q39, R40, and F41 of β-peptide (panel **C**) form a β-strand antiparallel to strand β5 of FLN. **D**, **E** Magnified view of the active site with tetrahedral coordination of the zinc ion. The fourth coordinating atom is a water molecule (red sphere) in the α-peptide complex (panel **D**) and a carbonyl oxygen in the β-peptide complex (panel **E**). Distances in Å between the carbonyl carbon of the scissile bond and Q132 are labeled in gray. **F** Superimposition of complexes between the FLN and α-peptide and the FLN- β-peptide complex. The overlay was based on the C-half of FLN. N-half domains are shown as molecular surfaces colored in cyan (α-peptide complex) and gray (β-peptide complex). The linker and C-halves are shown as ribbons. FLN adopts a slightly more closed conformation when bound with the β-peptide ("C2") than in the α-peptide complex ("C1"), see text. **G** Magnified view of the FLN active site. The slightly more closed conformation in the β-peptide complex is accompanied by a shift in the position of the zinc ion toward the β-peptide.

inhibitor MK-4815 on the distribution of FLN molecules adopting either open or closed states.

The binding of the MK-4815 inhibitor shifts the equilibrium between an open and a partially closed conformation of falcilysin

Thus far, crystal structures have captured FLN in closed conformations ("C1" or "C2"). To capture an open form of FLN, we employed single-particle cryo-EM as grid vitrification is likely to freeze molecules in a variety of conformations, thus providing a reasonably accurate sampling of structures adopted by FLN in solution. Two data sets were collected: (i) free FLN and (ii) FLN preincubated with MK-4815 (Table 3). 2D classification followed by 3D reconstructions (Fig. 4A, B, Figs. S5 and S6) revealed that in both data sets, FLN molecules could adopt either an open or a partially closed ("pC") conformation described below. Remarkably, the ratio between the number of molecules adopting these two conformations appears reversed between these two data sets (Fig. 4C, D). Out of 556,773 particles selected after initial 2D & 3D classification in the free FLN data set, 385,133 particles are in the open conformation, and 171,640 particles are in the "pC" conformation (Fig. S5). Consistently, after 3D refinement, 101,660 particles are in the open conformation, and 50,355 particles are in the "pC" conformation (Fig. 4C, Fig. S5), also giving an open/pC ratio of about 2:1. In contrast, in the FLN-MK-4815 mixture data set, out of 257,766 particles selected after initial 2D & 3D classification, 88,926 particles are in the open conformation, and 168,840 particles adopt the "pC" conformation (Fig. S6). After final 3D refinement, 45,566 particles are in the open conformation, and 98,298 particles are in the "pC" conformation (Fig. 4D, Fig. S6), giving a reversed open/pC ratio of about 1:2.

Cryo-EM maps of the open and "pC" conformations adopted by FLN when frozen on the grids are displayed in Fig. 4C, D and a summary of structural parameters characterizing the open and the three closed conformations of FLN, "pC", "C1", and "C2" is given in Table 2. Compared to the "PC" conformation, the "open" state results from an outward rotation by approximately 27° of one-half domain with respect to the other

(Supplementary Video 1). The rotation axis runs approximately midway through the cavity between the two domains (Fig. 4E). This rotation movement results in the full opening of FLN to substrates, giving the largest inter-domain distance of approximately 25 Å at one extremity of the molecule (Fig. 4E). At the other end of the molecule, the position of helix α13 in the N-half spanning residues 499–518 remains largely unaffected, when either the N-half or C-half is used for superimposition between the open and "pC" structures (Fig. 5A). As this helix lies along the rotation axis, it was therefore termed 'hinge helix'. Nonetheless, a small but noticeable movement of helix α13 accompanies this opening movement. In addition, a movement of the linker compensating for the change in the relative position between N-half and C-half is observed.

Figure 4F shows a comparison between the "pC" closed conformation and the closed conformation "C1" of FLN (identified using X-ray crystallography). Having overlapped C-half domains, a residual rotation of about 4° is needed to bring the N-half domains in coincidence (structural parameters are detailed in Table 2).

Of note, the FLN open conformation is highly similar between the two cryo-EM data sets with an overall r.m.s deviation of 0.45 Å. Likewise, at the resolution of the reconstruction obtained for the partially closed structures (pC), its structure in the free FLN dataset is indistinguishable from pC in the dataset where FLN was incubated with MK-4815. In the latter data set, strong electron density for MK-4815 was found only in molecules adopting the "pC" conformation, while only background electron density was observed at the corresponding location in molecules adopting the open conformation (Fig. 4D). An attempt to fit MK-4815 into the electron density of molecules having the open conformation led to too close contacts (1.7 Å) between the inhibitor and residues I513 and L514 (Fig. 4D inset). In contrast, in the "pC" conformation seen in the FLN-MK-4815 mixture (Fig. 4D), MK-4815 was fitted into density confidently without steric clash and with the same binding orientation as in the FLN-MK-4815 crystal structure[11]. Taken together, we conclude that the binding of MK-4815 shifts the equilibrium in the distribution of FLN molecules by promoting the formation of the partially closed "pC" conformation of FLN. This conclusion is supported by (i) the shift in the open/pC ratio of FLN molecules adopting either the open form or the "pC" state following the addition of MK-4815 to obtain the mixed data set and (ii) the observation of a very similar binding mode of MK-4815 to FLN in both the crystal structure and in the cryo-EM derived complex with the inhibitor.

The MK-4815 binding pocket is altered during the transition between the open and partially closed conformations of falcilysin

As the MK-4815 binding pocket is located next to helix α13, its shape can be affected by even slight movement of this hinge helix. As seen above, MK-4815 was excluded from the binding pocket when FLN adopts its open conformation, due to steric hindrance. In contrast, MK-4815 could bind to FLN in its "pC" state (Fig. 5A). In turn, incubation with and binding of MK-4815 affects the equilibrium between the various conformations adopted by FLN in solution, by shifting the population to a majority of FLN molecules having the pC conformation and depleting the population with an open state.

During the transition from the "pC" to the open conformation, the interdomain rotation opens one side of FLN and decreases inter-domain distance on the other side (Fig. 5A, B). As a result, the C-half is shifted toward the hinge helix (Fig. 5A). In particular, I739 in the C-half is displaced by a distance of 4.7 Å towards the position occupied by the side chain of K515 in the "pC" conformation. In turn, the sidechain of K515 rotates by an angle of 60° and shifts by 1.8 Å, leaving room for residue I739 (Fig. 5C). Of note, while in the "pC" conformation, I513 is 3.6 Å away from MK-4815, the distance is reduced to 2.5 Å in the open conformation. Thus, MK-4815 preferentially binds to FLN in its "pC" conformation and hinders the movement of the hinge helix that accompanies the "pC"-to-open state transition of FLN.

Table 2 | Structural comparison between the open, "C1", "C2" and partially closed "pC" structures

State	PDB code	R.m.s deviation based on C-half superimposition (Å)		R.m.s deviation based on N-half superimposition (Å)		Opening angle (°)
		N-half	α13	C-half	α13	
C1	8WXW	N.A.[a]	N.A.	N.A.	N.A.	1.0
C1	3S5H	0.67	0.76	0.68	0.53	2.3
C1	3S5I	0.59	0.71	0.55	0.56	2.2
C1	3S5M	0.55	0.71	0.55	0.50	2.3
C1	7DI7	0.50	0.28	0.48	0.27	2.2
C1	7DIA	0.53	0.28	0.36	0.24	1.6
C1	7DIJ	0.39	0.46	0.31	0.37	1.2
C1	7VPE	0.37	0.37	0.30	0.26	1.6
C1	8HO4	0.64	0.44	0.67	0.36	2.1
C1	8HO5	0.49	0.27	0.28	0.24	2.0
C2	8WXZ	1.60	0.55	1.76	0.53	−3.4
C2	3S5K	1.44	0.76	1.49	0.68	N.A.[b]
pC	8WYX	1.97	0.71	2.30	0.85	5.2
pC	8WYT	1.97	0.71	2.30	0.85	5.2
open	8WYY	19.0	4.29	17.3	1.53	32.5
open	8WYU	18.9	4.17	17.2	1.44	32.8

[a]FLN-α peptide complex (this work, PDB code: 8WXW) was used as the reference for superposition.
[b]K217 of PDB 3S5K is disordered.
R.m.s deviations were calculated for the N- or C-half Cα atoms between different conformations. Smaller yet noticeable changes in hinge helix α13 are also presented. Opening angles between the N-halves and C-halves are quantified by measuring the K217–E516–P1069 angle. A negative angle value denotes an opening between the two half domains in the opposite direction.

Discussion

Here using two human hemoglobin peptides of 14 and 15 amino acids, derived from α and β chain, respectively, we studied the molecular basis for substrate recognition and cleavage by FLN, a key event providing amino acids for the parasite metabolism. Sequence conservation and a shared mode of binding between the two hemoglobin peptides suggest that these structures represent a good model for hemoglobin cleavage by FLN. However, it is not known whether they depict accurately how FLN recognizes sequences from apicoplast proteins that are digested by FLN. To solve this issue, we attempted to co-crystallize FLN E132Q inactive mutant with a peptide having the apicoplast sequence: "FKNTQKDGVSL/QILKK/K/RSNQVNF" derived from a 24-residues ACP transit peptide[20], where "/" indicates the putative cleavage sites. However, co-crystallization with this peptide only gave free FLN crystals, although previously reported mass spectrometry results proposed that FLN could cleave ACP transit peptide[20]. Preferred amino acids at positions ranging from P5 to P5' for optimal FLN activity were systematically studied and the current data give a 3D explanation for these substrate preferences[16]. These structures give the first structural insights, to our knowledge, into the interaction between FLN and hemoglobin peptides which are well-documented biological substrates of FLN. Specificity results from an extensive set of interactions between α-peptide Y42 at P1' (F41 in the β-peptide) with FLN, providing a structural explanation for the preference of tyrosine and phenylalanine at the P1' position reported previously[16]. This is consistent with the observation that the P1' position constitutes the major determinant of metalloprotease specificity[18]. The requirement of residues at other positions appears less stringent, although P2 and P1 are polar or charged in the example reported here.

Both peptide substrates interact extensively with residues from both N-half and C-half of FLN. Such interactions are likely to favor a closed conformation as a result of peptide substrate binding. In contrast, after proteolysis, two shorter peptide products occupy the catalytic chamber,

Table 3 | Cryo-EM data collection, processing, and structure refinement

Data sets	Free falcilysin		Falcilysin + MK-4815	
Conformations	Open (EMD-37941) (PDB 8WYY)	Partially closed (EMD-37940) (PDB 8WYX)	Open (EMD-37939) (PDB 8WYU)	Partially closed (EMD-37938) (PDB 8WYT)
Data collection and processing				
Magnification	215,000		215,000	
Voltage (kV)	300		300	
Electron exposure (e–/Å^2)	40		40	
Defocus range (μm)	−2.5 to −0.5		−2.5 to −0.5	
Pixel size (Å)	0.573		0.58	
Symmetry imposed	C1		C1	
Initial particle images (no.)	385,133	171,640	88,926	168,840
Final particle images (no.)	101,660	50,355	45,566	98,298
Map resolution (Å)	3.1	3.5	3.2	2.7
FSC threshold = 0.143				
3D-FSC sphericity	0.863	0.778	0.770	0.864
Refinement				
Initial model used (PDB code)	3S5M	3S5M	3S5M	3S5M
Model resolution (Å)	3.12	4.17	3.43	2.77
FSC threshold = 0.5				
Map sharpening *B* factor (Å^2)	−79.48	−101.68	−75.98	−66.33
Model composition				
Non-hydrogen atoms	8795	8809	8819	8826
Protein residues	1069	1070	1072	1070
MK-4815	0	0	0	1
Zinc	1	1	1	1
B factors (Å^2)				
Protein	109.09	156.03	116.19	83.47
MK-4815	N.A.	N.A.	N.A.	68.72
Zinc	162.00	175.20	158.98	137.20
R.m.s. deviations				
Bond lengths (Å)	0.007	0.005	0.006	0.006
Bond angles (°)	0.746	0.569	0.808	0.574
Validation				
MolProbity score	1.90	1.72	2.07	1.70
Clashscore	12.64	10.00	18.85	9.82
Poor rotamers (%)	0.20	0.20	0.51	0.20
Ramachandran plot				
Favored (%)	95.85	96.80	95.77	96.89
Allowed (%)	4.05	3.20	4.23	3.11
Disallowed (%)	0.09	0.00	0.00	0.00

each of which interacts almost exclusively with either the N-half or C-half domain of FLN, thus releasing constraints favoring the closed conformation. Consequently, in the absence of inhibitors, following proteolysis, FLN can open up again, allowing the release of the peptide products and the initiation of a new catalytic cycle.

Human presequence protease (hPreP) is another mitochondrial M16C metalloprotease, that shares only 23% amino-acid sequence identity with FLN and was recently captured in multiple conformations, including an open state and several closed conformations[26]. A side-by-side structural comparison between FLN and hPreP reveals conserved overall architectures (Fig. 6): both 3D structures consist of an N-terminal half, a C-terminal half, and a linker connecting the two halves in a flexible manner. Following superimposition of 775 Cα atoms, the two open structures of FLN and hPreP differ by an r.m.s deviation of 2.2 Å (Fig. 6A) and the two closed structures by an r.m.s deviation of 1.9 Å over 744 Cα atoms (Fig. 6B). Most importantly, a hinge helix is present in both FLN and hPreP enzymes and known allosteric inhibitors bind in a pocket next to it (Fig. 6B). Consistently, this hinge helix was called "switch B" in hPreP and was proposed to mediate the open to closed transition of hPreP[26], in a manner consistent with what we propose here for FLN.

However, some noticeable differences do exist between FLN and hPreP: Free FLN particles preferentially adopt an open conformation as shown in this study, while free hPreP particles (74%) are mostly found in a "partially open conformation". The latter corresponds to a nearly closed conformation[26]. Moreover, the two proteins share only low sequence identity and behave differently in solution: Prep-C is denatured during the vitrification process[26]. In contrast, no denaturation issue during vitrification was observed for FLN. Taken together, these differences suggest the existence of a common ancestor for both metalloproteases. During evolution, a significant degree of divergence between FLN and hPreP was introduced, suggesting that inhibitors of one enzyme might not be effective against the other despite an overall conserved mode of action.

Several insightful biochemical and structural studies on the M16 family of zinc metalloproteases have been published, and some of the earlier studies already reported that conformational dynamics plays a crucial role in the functions of these enzymes[18,19,23–26]. In this study, we observed three closed conformations adopted by FLN: two closed conformations ("C1" and "C2") were trapped using X-ray crystallography, and one partially closed conformation, "pC", was observed using cryo-EM-based reconstructions. While the "pC" conformation might act as an intermediate between the closed and open conformations, we cannot completely rule out that the structural difference between the pC and closed conformations are an artifact originating from the various structure determination techniques employed: cryo-EM vs crystallography. To allow for substrate binding and product release, FLN needs to adopt an open conformation[11] for which a structure was hitherto lacking. The question has been answered in this study leading to the identification of a hinge region between the N-half and C-half of FLN, next to the inter-domain linker (Fig. 4E). During the opening of the enzyme, the two halves rotate along the hinge, resulting in a final opening angle of approximately 32.5° and an inter-domain distance of approximately 25 Å, large enough for peptide entry and exit. While the N-half and C-half are covalently connected by the linker, they also appear to interact with each other noncovalently through residues near the hinge.

The observation of a partially closed "pC" conformation of FLN captured in cryo-EM was a surprise as it was previously not described. Being slightly more open than the "C1" conformation (Fig. 4F), the "pC" conformation might constitute a metastable intermediate between the closed conformations ("C1" and "C2") and the open conformation. In this scheme, upon cleavage of the peptide substrate, FLN would first transition from the closed conformations into the "pC" conformation before opening up further into the fully "open" conformation.

Although the promiscuous allosteric pocket in FLN appears as "druggable" as it leads to enzymatic inhibition, for instance, after MK-4815 binding, as demonstrated here, a direct causal link with the mode of action in killing the parasite could not be established unequivocally for several drugs and thus constitutes a limitation of our studies[11]. Nonetheless, this study has provided detailed experimental evidence for the putative allosteric mode of inhibition that was proposed earlier, and that can, in principle, be exploited to design more potent inhibitors of FLN. This mode of action for FLN

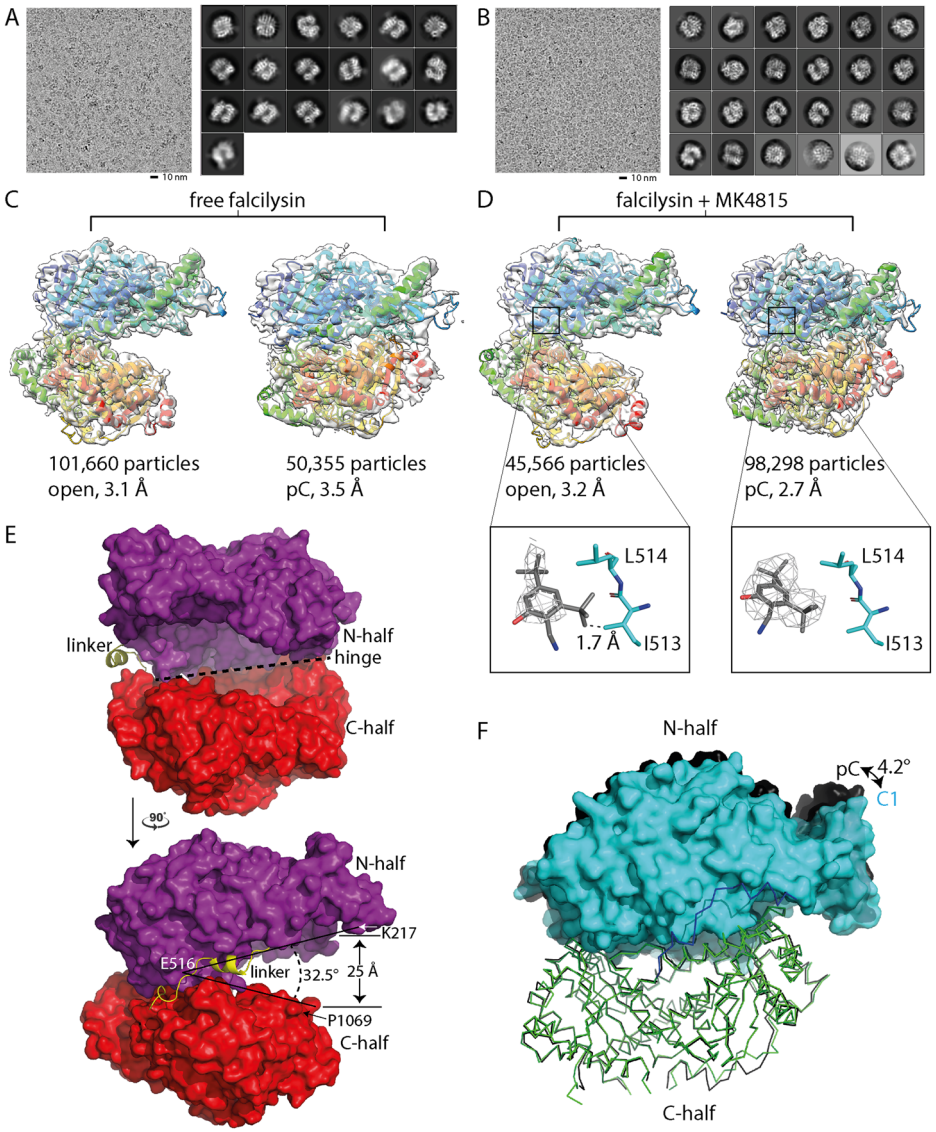

Fig. 4 | Cryo-EM reconstructions of Falcilysin in the presence and absence of MK-4815. A Raw micrograph and 2D classes of free FLN particles. **B** Raw micrograph and 2D classes of MK-4815-treated FLN particles. **C** Falcilysin 3D reconstructions in the absence of MK-4815. A majority of FLN particles are in the open conformation, and a minority are in the partially closed ("pC") conformation. FLN structures are colored in "rainbow colors" from N- (blue) to C-terminal end (red), with transparent cryo-EM electron density maps overlaid. **D** Falcilysin 3D reconstructions in the presence of MK-4815. A majority of FLN particles adopt the partially closed conformation ("pC"), and a minority in the open conformation. Cryo-EM electron density map for FLN preincubated with MK-4815 are displayed at 3σ (lower panels). In the open conformation, fitting MK-4815 resulted in too close contact with the side chain of I513 and L514. Moreover, the map at position MK-4815 is weak, suggesting only very low occupancy. In the partially closed conformation, MK-4815 has strong density, and fitting MK-4815 introduces no steric hindrance with nearby residues. **E** Falcilysin open structure displayed as a molecular surface. N-half: purple, C-half: red. Linker: yellow ribbon. The dotted line depicts the hinge axis between N-half and C-half. **F** Superimposition of the partially closed conformation ("pC" obtained in the cryo-EM reconstructions) and the closed conformation ("C1" obtained using X-ray crystallography with the α-peptide). The overlay is based on C-halves. N-halves are shown as molecular surfaces. Linkers and C-halves are shown as ribbons. When in its "pC" state, FLN adopts a slightly more open conformation than in the "C1" state (please see text).

inhibition by MK-4815 and by other compounds, such as quinolines, that bind to the same pocket is illustrated in Fig. 7 and outlined below.

In the absence of inhibitors or substrates, FLN preferably adopts an open conformation with a minor population of FLN molecules in the closed conformation. Binding of an allosteric inhibitor such as MK-4815 causes FLN to close up by inducing a movement of the hinge helix (Fig. 7A), thus reducing the available population of enzymes in the open conformation able to enter the catalytic cycle (Fig. 7B–E) as only the open conformation allows diffusion of the substrate (Fig. 7C). Upon substrate binding, interactions with both N-half and C-half induce closure of FLN (Fig. 7D). Next, substrate hydrolysis produces two shorter peptides no longer covalently linked, thus weakening the substrate-mediated interactions between N-half and C-half (Fig. 7E). As a result, FLN can open up and products are released, leading to the start of the next catalytic cycle (Fig. 7B).

The binding of MK-4815 is unlikely to compete with substrate binding (Fig. S7C) and might help to induce the closed conformation (Fig. S7D). Given the long distance from the zinc ion, MK-4815 is also unlikely to exert any direct effect on the hydrolysis reaction. Besides sequestering FLN molecules and preventing them from entering the catalytic cycle (Fig. 7A), MK-4815 could also exert its inhibitory effects by another mean (Fig. S7): by inhibiting the last step of the catalytic cycle: the transition from the closed to open conformations needed to allow the release of the products. This transition requires coordinated movement of the hinge helix, which results in a steric clash with MK-4815, and hence is hindered by MK-4815 binding (Fig. S7E). In summary, MK-4815 is an allosteric inhibitor that likely works both by (i) sequestering FLN molecules in a closed state and preventing them from entering the catalytic cycle (Fig. 7A) and (ii) by slowing down the release of the products trapped in the FLN catalytic chamber in the post-cleavage closed state (Fig. S7E).

In addition to MK-4815, we previously reported four other inhibitors of FLN and captured FLN-inhibitor complex crystal structures in the "C1" closed conformation[11] (MMV000848, PDB accession number: 8HO4; MMV665806, 8HO5; mefloquine, 7DIA; chloroquine, 7DI7). These four inhibitors bind to the same allosteric pocket as MK-4815, next to the hinge helix. It is, therefore, likely that these inhibitors also function by trapping FLN in a closed conformation. Consistent with this hypothesis, when N-halves of the open conformation and the FLN-inhibitor complex structures are structurally aligned, we observe steric clashes between the inhibitors and the open FLN, due to the movement of I739 and the hinge helix when transitioning from the closed to open conformations (Fig. S8).

In conclusion, we have identified a mechanism accounting for an allosteric mode of FLN inhibition that can be used to design more potent drugs that could be used as antimalarials.

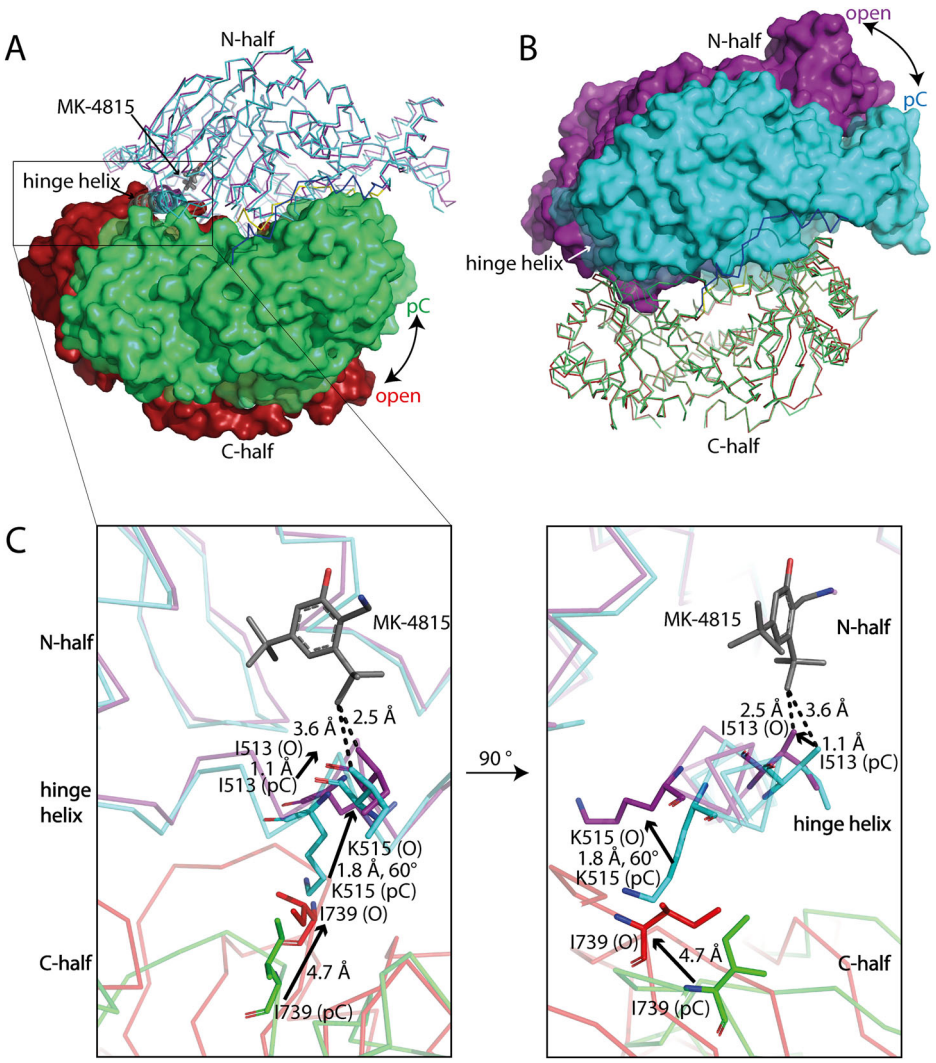

Fig. 5 | Structure of falcilysin in its open and partially closed conformations. A, **B** Structure alignment based on N-halves (panel A) or C-halves (panel B). The partially closed "pC" conformation of FLN is colored in cyan (N-half), blue (linker), and green (C-half); the open conformation of FLN is colored in purple (N-half), yellow (linker), and red (C-half). Rotations of N-half and C-half when transitioning from open to "pC" states are indicated by double-headed arrows. MK-4815 binds to the N-half domain in "pC" conformation next to the hinge helix α13, which makes direct contact with the C-half domain. **C** Magnified views of the hinge helix from two orthogonal directions. The open and "pC" conformations are aligned based on N-halves and displayed as ribbons following the same color code as in panel (**A**). During the transition from the "pC" to open conformations, I739 moves towards the position occupied by the K515 side chain in the "pC" state. As a result, the hinge helix is shifted toward the binding pocket of MK-4815. In the "pC" conformation, I513 is 3.6 Å away from MK-4815. In the open conformation, I513 would be too close to MK-4815, causing steric hindrance. Thus, the binding of MK-4815 disfavors open conformation (see text).

Materials and methods

Falcilysin cloning, expression, and purification

The procedures for wild-type FLN have been described previously[11]. The N-terminal 58 residues of FLN, which probably contain a signal peptide[17], were excluded in the recombinant protein design, and the final construct only contains the mature form of FLN. Alternatively, FLN was proposed as a peripheral membrane protein[16] which might be the role played by the N-terminal 58 residues.

Residue 59–1193 of the FLN gene, denoted as Q76NL8 in UniProtKB with a corresponding gene ID of 814283, was synthesized and incorporated into the pNIC28-Bsa4 vector downstream of a 6xHis tag and a TEV cleavage site, resulting in the construction of pNIC-FLN59-1193. This was achieved through ligation-independent cloning (LIC), utilizing a forward primer (5′-TACTTCCAATCCATGGAGTGGATACATGAG-3′) and a reverse primer (5′-TATCCACCTTTACTGTCATTCTATTAATACCTTTTTAAATTC-3′). Following the transformation of BL21 (DE3) Rosetta T1R cells with pNIC-FLN59-1193, cultivation was conducted at 37 °C until the optical density at 600 nm (OD_{600nm}) reached 0.6. Induction of protein expression was accomplished by supplementing the culture with 0.5 mM IPTG for a duration of 16 hours at 16 °C. Bacterial harvesting was carried out through centrifugation, and subsequently, cells were resuspended in a solution comprising 100 mM Na HEPES, 500 mM NaCl, 10 mM Imidazole, 10% (v/v) glycerol, 0.5 mM TCEP, at a pH of 7.5. Mechanical lysis was performed using an LM20 microfluidizer, and the resultant lysate was clarified by centrifugation at 50,000*g* for 1 h. Protein purification was executed through affinity chromatography utilizing Ni-NTA beads (GE Healthcare), with elution performed in a buffer consisting of 20 mM Na HEPES, 500 mM NaCl, 500 mM Imidazole, 10% (v/v) glycerol, 0.5 mM TCEP, at a pH of 7.5. Subsequent size exclusion chromatography employed a Hiload 16/600 Superdex 200 pg column (GE Healthcare), equilibrated in a buffer comprising 20 mM Na HEPES, 300 mM NaCl, 10% (v/v) glycerol, 0.5 mM TCEP, at a pH of 7.5. The purity of the protein was assessed through SDS-PAGE prior to a concentration to 22 mg mL^{-1}. The concentrated protein was then flash-frozen and stored at −80 °C until its utilization. The FLN mutants were generated by site-directed mutagenesis and subsequently confirmed by DNA sequencing. The expression and purification of the mutants were performed following the procedures used for the wild-type falcilysin.

Co-crystallization, X-ray diffraction data collection, data processing, and structure solution

The hemoglobin α chain peptide (LSFPTTKTYFPHFD) and the hemoglobin β chain peptide (VVYPWTQRFFESFGD) were ordered from GenScript's custom peptide synthesis service, with purities exceeding 98%. Mixtures of recombinant falcilysin E132Q mutant protein at 19 mg mL^{-1} (141 μM) and either the hemoglobin α chain peptide or the hemoglobin β chain peptide at 400 μM were incubated on ice for 10 minutes, prior to crystallization screen with commercial kits (JCSG-plus™ & Morpheus from Molecular Dimensions; Index & PEG/Ion Screen™ from Hampton Research) using a mosquito crystallization

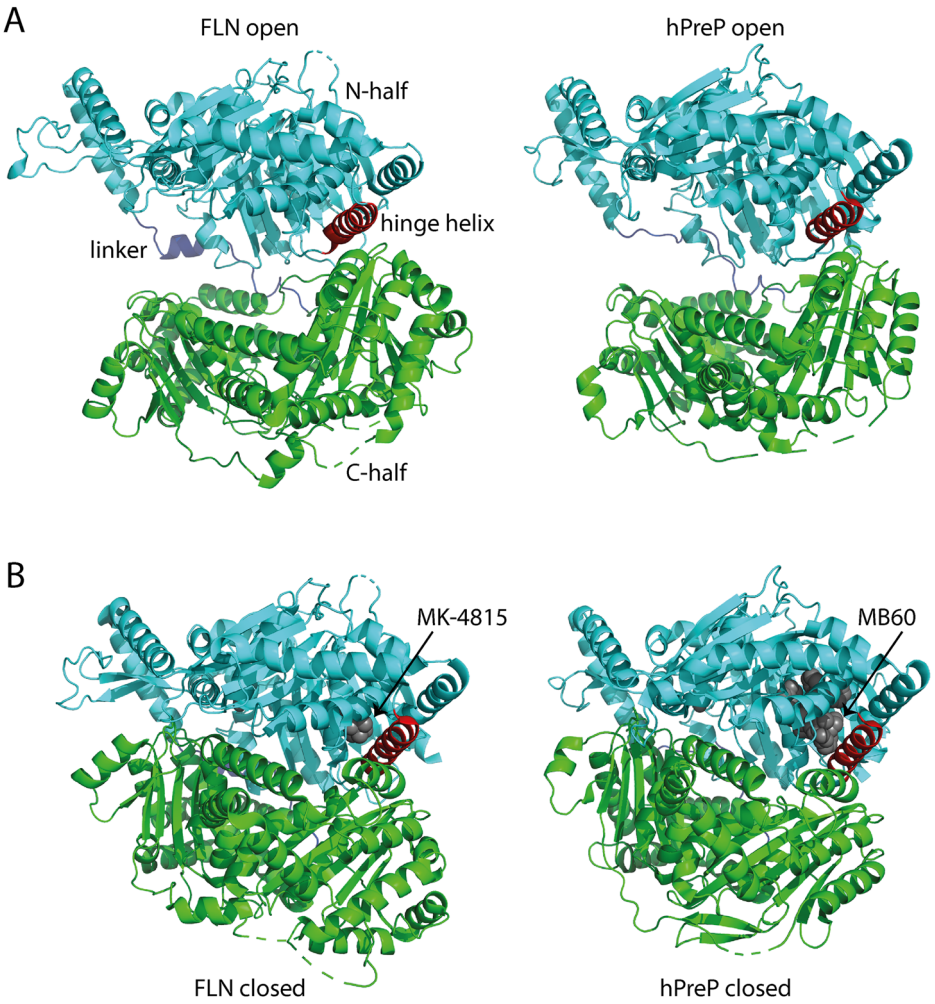

Fig. 6 | Comparison of the open conformation of falcilysin and human presequence protease. A The open conformation of FLN displayed as ribbons (this work, PDB accession number: 8WYY) and hPreP (PDB accession number: 6XOU); N-half are colored in cyan; C-half: green; hinge helix: red; linker region of FLN: purple. Disordered regions are indicated by dashes. **B** Closed conformation of FLN (this work, PDB accession number: 7DIJ) and hPreP (PDB accession number: 4RPU). The same color code as in panel (**A**) is used. Both allosteric inhibitors MK4815 (this work) and MB60 (PDB code: 4RPU) are displayed as gray spheres and bind next to the hinge region, impeding the dynamics of the metalloprotease.

robot (TTP Labtech). After 15 days, rod-like crystals were observed for the falcilysin α-peptide complex in JCSG-plus™ D1 well (24% w/v PEG 1500 and 20% v/v glycerol) with a protein-to-buffer ratio of 1:1, and for the falcilysin β-peptide complex in Morpheus F1 well (0.12 M monosaccharides, 0.1 M imidazole/MES monohydrate pH 6.5, 20% v/v PEG 500 and 10% w/v PEG 20000) with a protein-to-buffer ratio of 1:2. Crystals were fished and flash-frozen in liquid nitrogen, followed by shipment to Australian synchrotron beamline MX II where X-ray diffraction intensities were collected at a wavelength of 0.9537 Å. Next, data integration and scaling were performed using XDS[27], followed by molecular replacement using Phenix Phaser[28] with the free falcilysin structure as the search probe (PDB accession code: 3S5M). Subsequently, model refinement was performed by phenix.refine[29] interspersed with manual adjustment in COOT[30]. Finally, peptides were manually built into the active-site electron densities that could not be explained by falcilysin residues, followed by automatic refinement via phenix.refine. The Ramachandran plot analysis for the α-complex shows that 97.67% of the dihedral angles are in the favored regions, 2.33% are in the allowed regions, and there are no outliers. For the β-complex, 97.21% of the dihedral angles are in the favored regions, 2.79% are in the allowed regions, and there are no outliers, indicating that both structures have high stereochemical quality. F_o-F_c omit maps were generated by refinement with the peptides omitted. Data collection and refinement statistics are shown in Table 1. Residues V375-S403, N699 to T721, and N966 to V977 in the complex between FLN and the α-peptide are flexible. Likewise, residues V375-S406, K698-D715, and N966-M978 are flexible in the FLN β-peptide complex.

Cryo-EM data collection, processing, and model building

Both the free recombinant falcilysin wild-type protein at 0.5 mg mL^{-1} (3.7 μM) and the falcilysin-MK-4815 mixture consisting of the recombinant falcilysin wild-type protein at 0.5 mg mL^{-1} (3.7 μM) and MK-4815 at 50 μM were incubated on ice for 10 min, prior to application to cryo-EM grids. Quantifoil holey carbon-coated 300 mesh copper R 1.2/1.3 grids were glow-discharged for 1 min before mounting to Vitrobot tweezers. Four microlitres of the free falcilysin or falcilysin-MK-4815 mixture at 0.5 mg mL^{-1} was applied to the cryo-EM grids and blotted for 5 s with blot force 1 at 4 °C and 100% humidity using Vitrobot, followed by plunge-freezing in liquid ethane and transfer into liquid nitrogen. Images were obtained on a Titan Krios microscope (FEI) operated at 300 keV with Falcon 4i Direct Electron Detector (Thermo Fisher Scientific, USA), with automatic data acquisition using EPU following collection parameters as shown in Table 3.

Data processing was performed using RELION 3.1[31] (see workflow in Figs. S5 and S6). The dose-fractionated image stacks were subjected to beam-induced motion correction, followed by contrast transfer function (CTF) estimation by CTFFIND4[32]. For the MK-4815 treated data set, the selection of 961,731 particles from 6764 micrographs was done by autopick via the Laplacian of Gaussian (LoG) method, and particles were extracted with data binned by a factor of 2 (box size 128 and pixel size 1.16 Å). Contaminants and bad particles were discarded after reference-free 2D classification and initial 3D classification (257,766 particles left). After 3D refinement and classification, particles were separated into closed-form (168,840) and open-form (88,926 particles). In each state, particles with low resolution of either closed-form or open-form were excluded after 3D classification. Selected particles from each population were subjected to

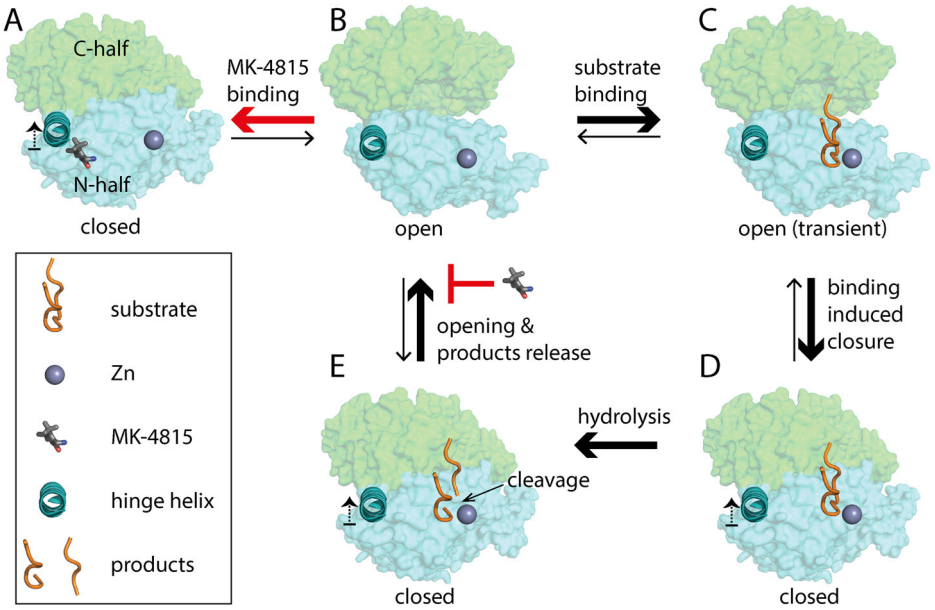

Fig. 7 | Proposed mechanism of FLN inhibition by MK-4815. A MK-4815 preferentially binds to FLN in a closed conformation, thereby restricting the movements of its hinge helix and preventing transition to an open conformation. **B** As a result, in the presence of MK-4815, only a minority of FLN molecules adopt an open conformation and are available for catalysis. **C** When FLN is in an open conformation, its peptide substrates are able to diffuse into the catalytic chamber, leading to a transient complex between the open state of FLN and the substrate. **D** Binding of the peptide substrate induces the closed conformation of FLN and a concomitant movement of the hinge helix. **E** Cleavage of the peptide substrate into products weakens the interaction between the N-half and C-half, allowing the opening of FLN and the release of proteolytic products. In the presence of MK-4815, the transition from the closed state "E" to the open state "B" is impaired and prevents FLN from re-entering the catalytic cycle after hydrolysis. The movements of the hinge helix, when the enzyme converts from open to closed conformations, are indicated by dashed arrows. The "favored" direction of the equilibria between different states is denoted by a large arrow, while the "disfavored" direction by a small arrow. For visualization, drawings are not to scale.

Bayesian polishing for per-particle, reference-based beam-induced motion correction.

Similarly, for the no-drug treated data set (free falcilysin), the selection of 2,511,554 particles from 18,180 micrographs was made by auto-pick via the LoG method, and particles were extracted with data binned by a factor of 2 (box size 128 and pixel size 1.146 Å). Contaminants and bad particles were discarded after reference-free 2D classification and initial 3D classification (leaving 171,640 particles of closed-form, and 385,133 particles of open-form). After 3D refinement and classification, particles with low resolution of either closed-form or open-form were excluded, and selected particles from each population were subjected to Bayesian polishing.

The binary masks were generated for the postprocessing procedure, and the resolution estimations were based on the gold-standard Fourier shell correlation (FSC) = 0.143 criterion[33]. The models of the N-half, C-half and linker were generated from the falcilysin crystal structure (PDB accession number: 7DIJ), and manually fitted to the maps in ChimeraX[34]. All models were subjected to Phenix real-space refinement and manually refined in COOT[30,35]. 3D-FSC sphericity values were calculated using the 3DFSC Processing Server (https://3dfsc.salk.edu/)[36]. FSC curves of 3D reconstructions and local resolution maps are included in Fig. S9.

Isothermal titration calorimetry

Isothermal titration calorimetry (ITC) was performed using a MICROCAL PEAQ-ITC instrument (Malvern) operated at 25 °C, with 500 rpm stirring speed in a buffer containing 50 mM sodium acetate, 300 mM NaCl, 0.5 mM TCEP, and 0.2% (v/v) DMSO. The α-peptide (LSFPTTKTYFPHFD) or β-peptide (VVYPWTQRFFESFGD), at a concentration of 200 µM, was titrated into 20 µM of the FLN mutants. The titration process was started with an initial injection of 0.4 µL over 0.8 s, followed by 19 subsequent injections of 2 µL over 3 s each, with a spacing of 120 seconds between each injection.

Enzymatic assay

The enzyme activities of the wild-type FLN enzyme, E132Q single mutant, N161A single mutant, and R1043A single mutant were measured in a buffer containing 50 mM sodium acetate, 300 mM NaCl, 0.5 mM TCEP, and 0.2% DMSO, using fluorescently labeled α-peptide (Dabcyl-LSFPTTKTYFPHFD-Edans) or β-peptide (Dabcyl-VVYPWTQRF-FESFGD-Edans) as substrate. A TECAN 10 M plate reader, operated at 336 nm and 495 nm wavelengths for excitation and emission, respectively, was used to monitor FLN protease activity. The reaction was started with the automated addition of the enzyme (either wild-type FLN or one of the mutants) into the peptide substrate, and the reaction was followed for a total duration of 1 min. The initial velocity was determined automatically using Magellan® software provided by the manufacturer. The measurements were performed in triplicate in the presence of varying concentrations of the fluorescently labeled α-peptide or β-peptide. Background subtraction was performed by measuring the addition of buffer alone into a range of concentrations of peptides. FLN enzymatic activity was normalized after background subtraction.

Differential scanning fluorimetry

Differential scanning fluorimetry experiments were performed in a buffer containing 20 mM Na HEPES at pH 7.5, 300 mM NaCl, 5% (v/v) glycerol, and 1 mM TCEP with a total volume of 25 µL. To test the stabilization effect of MK-4815 on FLN, 5 µM wild-type recombinant FLN protein was incubated with 5× SYPRO orange dye and varying concentrations of MK-4815, followed by RFU measurement using CFX96 Touch Real-Time PCR Detection System (Bio-Rad) on the FRET channel at temperatures ranging from 25 °C to 95 °C. Subsequently, raw RFU values were exported and analyzed using the GraphPad Prism software to determine the melting temperatures (T_m) of FLN. To test the stabilization effect of hemoglobin peptides on FLN, the E132Q mutant was used instead of the wild-type enzyme, to prevent peptide cleavage by FLN. For this assay, a concentration of 5 µM recombinant FLN E132Q mutant protein was incubated with 5× SYPRO orange dye, and varying concentrations of α-peptide (LSFPTTKTYFPHFD) or β-peptide (VVYPWTQRFFESFGD), followed by RFU measurement from 25 °C to 95 °C.

Reporting summary

Further information on research design is available in the Nature Portfolio Reporting Summary linked to this article.

Data availability

Atomic coordinates and structure factors for the falcilysin-hemoglobin peptide complexes reported here have been deposited with the PDB (www.rcsb.org) with access codes 8WXW (FLN-α-peptide complex) and 8WXZ (FLN-β-peptide complex). Experimental cryo-EM Coulomb potential maps have been deposited with the EMDB with access codes EMD-37941, and EMD-37940 for the open (8WYY) and partially closed (8WYX) structures of free falcilysin and EMD-37939, EMD-37938 for the open (8WYU) and partially closed (8WYT) structures obtained in the presence of MK-4815 with the latter containing the bound inhibitor. Source data for enzymatic assay and DSF are included in Supplementary Data 1. All other data are available from the corresponding author upon reasonable request.

Received: 23 February 2024; Accepted: 22 August 2024;
Published online: 31 August 2024

References

1. World Health Organization. *World Malaria Report 2022*.
2. Hoffman, S. L., Vekemans, J., Richie, T. L. & Duffy, P. E. The march toward malaria vaccines. *Am. J. Prev. Med.* **49**, S319–S333 (2015).
3. Dondorp, A. M. et al. Artemisinin resistance in *Plasmodium falciparum* malaria. *N. Engl. J. Med.* **361**, 455–467 (2009).
4. Phyo, A. P. et al. Declining efficacy of artemisinin combination therapy against *P. falciparum* malaria on the Thai–Myanmar Border (2003–2013): the role of parasite genetic factors. *Clin. Infect. Dis.* **63**, 784–791 (2016).
5. Hovlid, M. L. & Winzeler, E. A. Phenotypic screens in antimalarial drug discovery. *Trends Parasitol.* **32**, 697–707 (2016).
6. Spangenberg, T. et al. The open access malaria box: a drug discovery catalyst for neglected diseases. *PLoS ONE* **8**, e62906 (2013).
7. Murithi, J. M. et al. Combining stage specificity and metabolomic profiling to advance antimalarial drug discovery. *Cell Chem. Biol.* **27**, 158–171.e3 (2020).
8. Allman, E. L., Painter, H. J., Samra, J., Carrasquilla, M. & Llinás, M. Metabolomic profiling of the Malaria Box reveals antimalarial target pathways. *Antimicrob. Agents Chemother.* **60**, 6635–6643 (2016).
9. Powles, M. A. et al. MK-4815, a potential new oral agent for treatment of malaria. *Antimicrob. Agents Chemother.* **56**, 2414–2419 (2012).
10. Dziekan, J. M. et al. Cellular thermal shift assay for the identification of drug–target interactions in the *Plasmodium falciparum* proteome. *Nat. Protoc.* **15**, 1881–1921 (2020).
11. Wirjanata, G. et al. Identification of an inhibitory pocket in falcilysin provides a new avenue for malaria drug development. *Cell Chem. Biol.* **31**, 743–759.e8 (2024).
12. Dziekan, J. M. et al. Identifying purine nucleoside phosphorylase as the target of quinine using cellular thermal shift assay. *Sci. Transl. Med.* **11**, eaau3174 (2019).
13. Chung, Z. et al. Identification and structural validation of purine nucleoside phosphorylase from *Plasmodium falciparum* as a target of MMV00848. *J. Biol. Chem.* **300**, 105586 (2024).
14. Eggleson, K. K., Duffin, K. L. & Goldberg, D. E. Identification and characterization of falcilysin, a metallopeptidase involved in hemoglobin catabolism within the malaria parasite *Plasmodium falciparum*. *J. Biol. Chem.* **274**, 32411–32417 (1999).
15. Murata, C. E. & Goldberg, D. E. *Plasmodium falciparum* falcilysin: an unprocessed food vacuole enzyme. *Mol. Biochem. Parasitol.* **129**, 123–126 (2003).
16. Murata, C. E. & Goldberg, D. E. *Plasmodium falciparum* falcilysin: a metalloprotease with dual specificity. *J. Biol. Chem.* **278**, 38022–38028 (2003).
17. Ralph, S. A. Subcellular multitasking—multiple destinations and roles for the *Plasmodium falcilysin* protease. *Mol. Microbiol.* **63**, 309–313 (2007).
18. Arolas, J. L., Goulas, T., Cuppari, A. & Gomis-Rüth, F. X. Multiple architectures and mechanisms of latency in metallopeptidase zymogens. *Chem. Rev.* **118**, 5581–5597 (2018).
19. Taylor, A. B. et al. Crystal structures of mitochondrial processing peptidase reveal the mode for specific cleavage of import signal sequences. *Structure* **9**, 615–625 (2001).
20. Ponpuak, M. et al. A role for falcilysin in transit peptide degradation in the *Plasmodium falciparum* apicoplast. *Mol. Microbiol.* **63**, 314–334 (2007).
21. Edgar, R. C. S. et al. Genetic and chemical validation of *Plasmodium falciparum* aminopeptidase PfA-M17 as a drug target in the hemoglobin digestion pathway. *Elife* **11**, e80813 (2022).
22. Loughlin, W. A., Tyndall, J. D. A., Glenn, M. P., Hill, T. A. & Fairlie, D. P. Beta-strand mimetics. *Chem. Rev.* **110**, PR32–PR69 (2010).
23. Shen, Y., Joachimiak, A., Rich Rosner, M. & Tang, W. J. Structures of human insulin-degrading enzyme reveal a new substrate recognition mechanism. *Nature* **443**, 870–874 (2006).
24. Johnson, K. A. et al. The closed structure of presequence protease PreP forms a unique 10 000 Å3 chamber for proteolysis. *EMBO J.* **25**, 1977–1986 (2006).
25. King, J. V. et al. Molecular basis of substrate recognition and degradation by human presequence protease. *Structure* **22**, 996–1007 (2014).
26. Liang, W. G. et al. Structural basis for the mechanisms of human presequence protease conformational switch and substrate recognition. *Nat. Commun.* **13**, 1–14 (2022).
27. Kabsch, W. XDS. *Acta Crystallogr. D* **66**, 125–132 (2010).
28. McCoy, A. J. et al. Phaser crystallographic software. *J. Appl. Crystallogr.* **40**, 658–674 (2007).
29. Afonine, P. V. et al. Towards automated crystallographic structure refinement with phenix.refine. *Acta Crystallogr. D* **68**, 352–367 (2012).
30. Emsley, P. & Cowtan, K. Coot: model-building tools for molecular graphics. *Acta Crystallogr. D* **60**, 2126–2132 (2004).
31. Scheres, S. H. W. RELION: implementation of a Bayesian approach to cryo-EM structure determination. *J. Struct. Biol.* **180**, 519–530 (2012).
32. Rohou, A. & Grigorieff, N. CTFFIND4: fast and accurate defocus estimation from electron micrographs. *J. Struct. Biol.* **192**, 216–221 (2015).
33. Chen, S. et al. High-resolution noise substitution to measure overfitting and validate resolution in 3D structure determination by single particle electron cryomicroscopy. *Ultramicroscopy* **135**, 24–35 (2013).
34. Pettersen, E. F. et al. UCSF ChimeraX: structure visualization for researchers, educators, and developers. *Protein Sci.* **30**, 70–82 (2021).
35. Adams, P. D. et al. PHENIX: a comprehensive Python-based system for macromolecular structure solution. *Acta Crystallogr. D* **66**, 213–221 (2010).
36. Tan, Y. Z. et al. Addressing preferred specimen orientation in single-particle cryo-EM through tilting. *Nat. Methods* **14**, 793–796 (2017).

Acknowledgements

This work was supported by grant NRF-CRP24-2020-005 to J.L., P.P., and Z.B and by Tier 1 grant RG28/22 from the Singapore Ministry of Education to J.L. X-ray diffraction data were collected on the MX II beamline at the Australian Synchrotron, part of ANSTO, that we gratefully acknowledge.

Author contributions

Jianqing L. performed the crystallography work, EM grid preparation, ITC experiments, and structural analysis; designed the experiments and prepared and revised the initial draft. X.Y. and Y.G. processed the cryo-EM data and assisted in the methodology. Z.C. performed the mutagenesis, enzymatic assay, and differential scanning fluorimetry experiments. C.W.L. assisted in EM grid preparation. A.El S. and J.L. provided help and advice with structural studies. E.V.P. assisted in cryo-EM data collection. P.P., Z.B., and J.L. were responsible for funding acquisition and project

conceptualization. J.L. supervised the project, designed the experiments, and helped with the paper writing.

Competing interests
The authors declare no competing interests.

Additional information
Supplementary information The online version contains supplementary material available at https://doi.org/10.1038/s42003-024-06774-6.

Correspondence and requests for materials should be addressed to Julien Lescar.

Peer review information *Communications Biology* thanks the anonymous reviewers for their contribution to the peer review of this work. Primary Handling Editors: Janesh Kumar and Dario Ummarino. A peer review file is available.